COBEM 2023 27TH INTERNATIONAL CONGRESS OF MECHANICAL ENGENEERING

ABCM Brazilian Society of Mechanical Sciences and Engineering
27th ABCM International Congress of Mechanical Engineering
December 04-08, 2023, Florianópolis-SC, Brazil

COB-2023-2151
ASSESSMENT OF MECHANICAL PERFORMANCE IN A PLATE HEAT EXCHANGER ENHANCED BY A THICKER REINFORCEMENT PLATE.

Giovani Silveira de Magalhães Martins
Kleber Vieira de Paiva
Jorge Luiz Goes Oliveira

Thermal Fluid Flow Group – T2F, Department of Mobility Engineering, Federal University of Santa Catarina, Joinville, SC, Brazil.
giovani.martins@t2f.ufsc.br
kleber.paiva@t2f.ufsc.br
jorge.goes@t2f.ufsc.br

Abstract. *Plate heat exchangers (PHEs) are commonly used in the oil and gas industry for their high thermal efficiency. However, the use of thin plates can lead to mechanical weaknesses and failures due to excessive deformations. To address these issues, manufacturers suggest incorporating a thicker reinforcing plate within the plate pack. This study aims to experimentally assess the mechanical behavior of a PHE with and without a 6 mm thick reinforcing plate. Testing involved 96 stainless steel 316L plates with a thickness of 0.6 mm, subjected to hydrostatic tests with single and double channel pressurization. Three configurations were examined: no reinforcing plate, a freely positioned reinforcing plate, and a locked reinforcing plate. Strain gauge analysis and modal analysis were conducted to evaluate stress distribution and vibration modes for each configuration. Results showed minimal alteration in stress distribution when using the thicker intermediate plate, whether free or locked. The reinforcing plate had no significant impact on modal response, as frequency response function curves remained similar. The first vibration mode consistently occurred around 500 Hz. Therefore, for heat exchangers with fewer than 100 plates and similar dimensions to the studied object, the use of an intermediate reinforcing plate is not justified based on the observed differences.*

Keywords: *Plate heat exchangers, reinforcing plate, stresses, displacements, vibration mode.*

1. INTRODUCTION

Economic considerations, space constraints, and high thermal efficiency are key factors driving the demand for advanced heat exchangers in various industries. In response to these requirements, plate heat exchangers (PHEs) have emerged as a practical solution since the 1930s, gaining widespread adoption in sectors such as food processing, pharmaceuticals, and oil and gas. PHEs have often been favored over traditional shell-and-tube heat exchangers due to their compact design and superior heat transfer performance(Kakaç et al., 2020; Shah and Sekuli, 2003).

The effectiveness and compactness of PHEs have stimulated research and development efforts aimed at optimizing plate geometries. Among the various designs available, gasket plate heat exchangers (GPHEs) have become the most prevalent configuration (Wang et al., 2007). GPHEs employ plates with a Chevron angle (β) to enhance heat transfer rates compared to alternative geometries and configurations. Furthermore, the assembly concept of GPHEs facilitates ease of cleaning, sealing, and maintenance. However, the limitations of GPHEs, particularly with regards to temperature and pressure, have restricted their application to moderate operating conditions, typically up to 200°C and 15 bar (Beckedorff et al., 2022; Wang et al., 2007). Consequently, GPHEs are widely employed in liquid-liquid processes that demand flexibility and high thermal efficiency (Hewitt et al., 1994).

Notwithstanding their excellent heat transfer performance, the mechanical strength of GPHEs is compromised by the use of thin plates, leading to failures associated with excessive plate deformations. These deformations arise from the temperature differentials and pressure differentials experienced between adjacent plates, resulting in gasket expulsion from the confined channels (Adolfsson, 2016; Ryden, L., 2003)

To address this issue and improve the mechanical robustness of GPHEs, manufacturers commonly recommend the use of reinforcing plates within the plate pack. These thicker intermediate plates are designed to enhance structural integrity and minimize deformation. The purpose of the present study is to experimentally investigate the mechanical behavior of a GPHE under two different configurations: with and without a 6 mm thick reinforcing plate. Stress analysis, and modal analysis will be conducted to evaluate the impact of the reinforcing plate on stress distribution, displacements, and vibration modes.

Understanding the mechanical behavior of GPHEs and the impact of reinforcing plates is pivotal for optimizing their design and ensuring reliable and efficient operation across diverse industrial applications. This research contributes to the broader field of heat exchanger design and offers insights about the performance and durability of GPHEs.

2. MATERIAL AND METHODS

2.1 Plate Heat Exchangers

The design of plate heat exchangers, including the plate geometries, dimensions, and corrugations, varies among manufacturers and is tailored to their specific industrial applications (Arsenyeva et al., 2021). The selection of plate types and arrangement within the package is determined by the trade-off between pressure drop and heat transfer rate. In a comprehensive literature review conducted by Zhang et al. (2015) the thermal performance of gasket plate heat exchangers (GPHEs) was thoroughly investigated. The study explored a range of process parameters and corrugation geometries, identifying their significant influence on improving the overall effectiveness of the device.

The plate heat exchanger studied in this paper consisted of a package of 96 plates, all of which were classified as "H" plates based on their β values (β = 60º). Figure 1 presents a photograph of plates investigated on this study. "H" plates, with β > 45°, offer higher heat transfer rates and higher pressure drops compared to "L" plates, which have lower pressure drops but lower heat exchange rates (Kakaç et al., 2020; Martins et al., 2022). According to Gut et al. (2004), the corrugations, in addition to increasing the thermal performance, also improve the mechanical resistance of the plates. The main dimensions and technical specifications of the evaluated heat exchanger as shown in Table 1.

Figure 1. (a) Photograph of GPHE plate with β = 60º

Table 1. Technical specifications of heat exchanger evaluated

	Symbol	***Heat Exchanger***	***Units***
Maximum Pressure	P_{max}	10	bar
Maximum Temperature	T_{max}	180	ºC
Number of plates (package)	n	96	-
Plate thickness	t	0.6	mm
Material	-	AISI 316L	-
Porthole diameter	D_p	4 / 101.6	" / mm
Channel Space	b	2.5	mm
Effective length	L_v	720	mm
Plate Width	L_w	355	mm
Initial Tightening	A	305	mm

2.2 Stainless Steel Properties

To conduct a structural assessment of the heat exchanger, the mechanical properties of 316L stainless steel outlined in ASME Section II – Part D were utilized (The American Society of Mechanical Engineers, 2015). This industry standard categorizes the recommended properties based on the final product's form. Specifically, the properties of 316L stainless steel in plate form (SA-240-F316L-S31603-16Cr–12Ni–2Mo Plate) were adopted as the reference point (see Table 2).

Table 2. Mechanical Properties of 316L stainless steel according to ASME Section II – Part D.

Properties	***Value***	***Units***
Young Modulus (*E*)	195	GPa
Poisson's ratio (ν)	0.31	-
Minimum Ultimate Tensile Strength (*UTS*)	485	MPa
Minimum Tensile Yield Strength (*TYS*)	170	MPa

2.3 Experimental Procedure

The aim of this study is to assess the mechanical behavior of a plate heat exchanger (PHE) through strain gauge and modal analysis. These evaluations will be performed in three different plate configurations, are as follows:

I. Stainless Steel 316L: 96 plates (HH96) with a thickness of 0.6 mm.
II. Stainless Steel 316L: 96 plates (HH96) with a thickness of 0.6 mm and a free 6 mm reinforcing plate.
III. Stainless Steel 316L: 96 plates (HH96) with a thickness of 0.6 mm and a locked 6 mm reinforcing plate

A 6 mm thick carbon steel structural reinforcing plate will be utilized in the heat exchanger configuration. To ensure effective sealing, four sealing rings will be inserted into the inlet connections, as illustrated in Figure 2a. The performance of the heat exchanger assembly with the reinforcing plate will be evaluated under two conditions: with the reinforcing plate in a loose state, maintaining a gap between the surrounding nuts and the plate (Figure 2b), and with the reinforcing plate securely fastened, with nuts tightened on both sides of the plate.

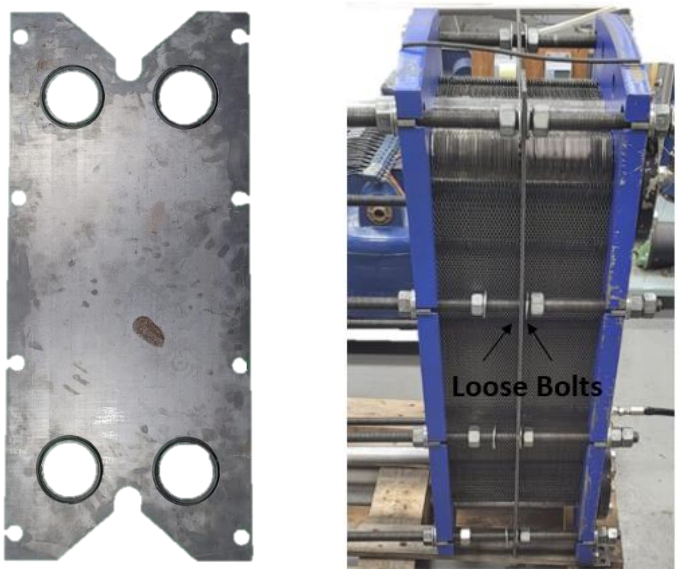

(a) (b)

Figure 2. (a) 6 mm thick carbon steel structural reinforcement plate. (b) Configuration II: Reinforcing plate in a loosened condition, maintaining a gap between the surrounding nuts and the plate.

Hydrostatic tests will be conducted in accordance with guidelines outlined in ASME Section VIII Division 2, Chapter 8.2, which recommends a maximum pressure of 1.43 times the service pressure of the heat exchanger. However, to thoroughly examine the PHE's mechanical performance and ensure its integrity, the tests will be conducted using the design pressure of 10 bar. To measure deformation during the hydrostatic tests, strain gauges will be utilized. The pressurization bench was designed by Flutrol Company and it aims at controlling cyclic pressure loads. The maximum allowed pressure is 20 MPa. The bench consists of a hydro-pneumatic pump, model ASF-35, fed by an air line at 7 bar, a

pressure relief system and valves which allow pressure control. Hydrostatic pressure loads are measured with a pressure transducer (PX401 Series Omega). The transducer measuring range is 0-5 MPa, and the uncertainty is 0.5 % of full scale.

The heat exchangers can operate under high pressures in either a single branch or double branch configuration. To represent these conditions, pressure testing procedures were conducted for both single branch (Single Test) and double branch (Double Test) configurations.

In the single hydrostatic pressure tests, one branch of the GPHE was pressurized with water while the other branch was exposed to the atmosphere. Triaxial strain gauges were strategically placed on the third plate's surface, which was in contact with air, to measure the strain. To prevent water contact, the cables, wires, and terminals were suitably protected.

For the double hydrostatic pressure tests, both sides of the heat exchanger were pressurized simultaneously. The branches were interconnected using an auxiliary hydraulic hose. In this test setup, a feedthrough connection was employed to transmit the strain signals to the data acquisition system. To ensure insulation and prevent water from coming into contact with the electrical connections, a specific silicone material recommended by the strain gauge manufacturer was applied.

3. STRESS DETERMINATION

The stress-strain diagram exhibits a linear relationship between stress and strain in the elastic region for most engineering materials. As a result, an increase in deformation (ε) leads to a proportional increase in stress (σ), characterized by Hooke's Law.

Triaxial cases, such as the one being discussed, require extended forms of Hooke's Law. Due to the geometric complexity of the PHE plate, deformation measurements will be taken in three directions (0°, 45°, 90°) to obtain the local stress state of the specimen:

$$\sigma_{p,q} = \frac{E}{2}\left[\frac{\varepsilon_0 + \varepsilon_{90}}{1-\nu} \pm \frac{\sqrt{2}}{1+\nu}\sqrt{(\varepsilon_0 - \varepsilon_{45})^2 + (\varepsilon_{45} - \varepsilon_{90})^2}\right] \quad (1)$$

Where ν is the Poisson's ratio and E is the modulus of elasticity. The subscripts 0°, 45°, and 90° refer to the deformation directions, while "p" and "q" refer to the principal stresses at the measurement point.

The von Mises criterion is used to determine the von Mises equivalent stresses, according to the equation below.

$$\sigma_{\mathrm{VM}} = \sqrt{\frac{\sigma_p^2 + \sigma_q^2 + (\sigma_p + \sigma_q)^2}{2}} \quad (2)$$

For the strain analysis of the heat exchanger, four triaxial strain gauges were installed at the critical points of interest. The strain gauges used were rosette type, with an R configuration and angles of 0°, 45°, and 90°, manufactured by Excel Sensores, model PA-09-060RB-120-L. Strain gauge SG1 was positioned at the center of the distribution region, SG2 on the unsupported diagonal, SG3 was placed near the nozzle, and SG4 in the thermal exchange region, as shown in Figure 3. It is important to note that these positions were determined following the procedures and methods described by (Martins et al., 2022).

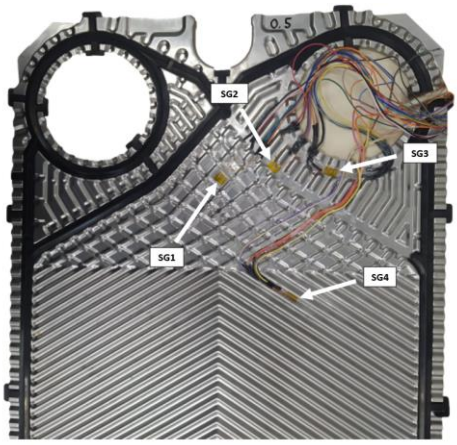

Figure 3. Positioning of triaxial strain gauges on the inner plate

Deformation uncertainty is 3% of the sensor full scale. Three NI 9237 modules and one NI-9203 module were applied as data acquisition systems for strain and pressure measurements, in that order. A NI cDAQ-9178 chassis was used for

simultaneous reading of each module. Uncertainties related to von Mises equivalent stresses were less 7% in hydrostatic tests.

4. MODAL ANALYSIS

Modal analysis of mechanical systems aims to determine the dynamic behavior of mechanical components/structures subjected to external dynamic loads. Based on the modal parameters of a mechanical system, which include natural frequencies, vibration modes, and damping factors, modal analysis seeks to describe the system's dynamics by capturing the effect of external loading on its steady-state response (Rao, 2004).

There are two approaches to conducting modal analysis: analytical and experimental. In many cases, especially for complex structures subjected to specific loading conditions or with unknown material properties and boundary conditions, it is challenging to obtain an accurate theoretical model that adequately reproduces the dynamic behavior of the structure, particularly when characterizing damping. In such cases, experimental modal analysis becomes an attractive approach. In this approach, a model of the structural dynamic properties is obtained by exciting the structure with measurable forces and determining the relationship between the structural response and the applied excitation (Prazzo, 2011; Nóbrega, 1996).

The tool that enables the description of the system's dynamics in relation to external loading is the frequency response function (FRF) matrix. The elements of the FRF matrix, which depend on the modal parameters and the frequency of the applied external loading, represent the relationship between the external loading and the steady-state response of the system (Rao, 2004).This cause-effect relationship describes the behavior as a function of frequency between two points on the structure. Therefore, if measurements of these transfer characteristics of the structure are taken, the structural dynamics are known, meaning that the properties defining a vibration mode can be obtained (Zahid et al., 2020)

Modal analysis is a process that involves fitting theoretical curves of an adopted model to experimental curves, thereby obtaining parameters that best approximate the set of experimental curves obtained. These parameters typically represent the modal characteristics of the system, as evident in the theoretical expressions of the frequency response functions (FRFs). The adjustment techniques used in this process are commonly referred to as modal identification techniques (Allemang and Avitabile, 2022; Maia and Silva, 2001)

Modal parameter identification techniques can be classified based on the domain (time or frequency) in which the experimentally obtained curves are processed, as well as the number of modes analyzed simultaneously, which can be either single-degree-of-freedom (SDOF) or multi-degree-of-freedom (MDOF). In the SDOF approach, only one mode can be analyzed at a time, assuming that the system behaves similarly to a single-degree-of-freedom system. On the other hand, the MDOF approach allows for the simultaneous analysis of multiple modes, but this technique can only be used in the time domain (Allemang and Avitabile, 2022; Jorge et al., 2022)

In the present procedure, an SDOF analysis based on peak identification was performed (Figure 4). This modal identification method is suitable for structures with well-separated modes and some damping. If this situation did not occur, imprecise measurements would be obtained in the vicinity of resonance. However, structures should not be excessively damped, so that the FRF in the vicinity of resonance is influenced by a single mode. This methodology is sometimes applied to obtain initial estimates of the modal parameters (Nóbrega, 1996).

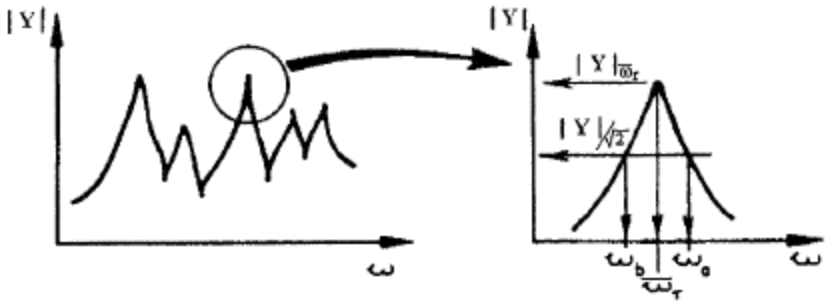

Figure 4. Peak identification (Nóbrega, 1996).

The frequency response function (FRF) with proportional damping can be expressed as:

$$Y_{jk}\,(\omega) = \sum_{r=1}^{N} i\omega . \frac{A_{jk}}{\overline{\omega}^2 - \omega^2 + i(2\omega\zeta_r\overline{\omega}_r} \tag{1}$$

Where $A_{jk,}$ c_r, $k_{r,}$ $\omega_{r,}$ ζ_r and m_r are: modal constant, modal damping coefficient, system stiffness coefficient, natural frequency of the mode under study, system damping and system mass, respectively. The method is applied as follows, using the aforementioned expression of the FRF:

1. Detect the peaks of the FRF magnitude, as shown in Figure 1, to isolate the modes to be identified. For each mode, identify the frequency at which the FRF magnitude is maximum, which corresponds to the natural frequency of the mode under study ($\bar{\omega}_{r)}$.
2. The maximum value of the FRF magnitude denoted by $|Y|_{\omega r}$ identifies the frequency range (D_ω) where the FRF magnitude is $|Y|_{\omega r}/\sqrt{2}$. The limits of this range, denoted as ω_a and ω_b, are known in the literature as "half power points" (see Figure 4).
3. The damping of the mode under study can be calculated using the following equation:

$$\zeta_r = \frac{\omega_a - \omega_b}{2\bar{\omega}_r} \tag{2}$$

4. An estimate of the modal constant for the mode in question can be obtained by assuming that the FRF at resonance is solely due to that mode. Substitute ω with $\bar{\omega}_r$ in the previous equation, yielding:

$$|Y| = \sum_{r=1}^{N} \frac{A_{jk}}{(2\zeta_r \bar{\omega}_r} \tag{3}$$

It should be noted that the accuracy of damping and modal constant estimation largely depends on the precision of the frequency response function (FRF) measurements, as this method primarily relies on FRF values. Additionally, most measurement errors are concentrated in the vicinity of resonance, particularly for lightly damped structures. Furthermore, this method only allows for obtaining real modal constants, resulting in real modes, i.e., structures with proportional damping. Another limitation of the method is its assumption of single-degree-of-freedom (SDOF) behavior, which is not always applicable. There may be cases where the modes are well separated, yet significant contributions from neighboring modes exist for the mode under study (Allemang and Avitabile, 2022; Nóbrega, 1996).

Experimental modal analysis can be divided into three distinct phases: test preparation, excitation and response measurement, FRF calculation, and modal parameter identification. Test preparation involves choosing the structural suspension/fixation method (boundary condition), the equipment and type of excitation, the measurement points on the structure, structure discretization, and the equipment used to measure excitation and response.

The tests were conducted in the typical operating configuration of the heat exchanger, with it being supported on the ground at its base. The heat exchanger consists mainly of the plate package, guide rod, fixed head, movable head, and reinforcement plate (if applicable). For modal analysis, impacts were performed in four situations, on the fixed head and the movable head.

The first procedure, of an exploratory nature, was carried out on the fixed head, with the accelerometer positioned on it and adopting 5 impact points. Each of the chosen points was impacted at least three times using a hammer equipped with a force transducer, with the accelerometer measuring the structure's acceleration at point 2, which remained fixed during all measurements. Thus, the force transducer in the hammer, responsible for measuring the excitation force of the structure, and the accelerometer, responsible for measuring the acceleration, allow for the calculation of the necessary frequency response functions (FRFs) to determine the natural frequencies (eigenvalues) and vibration modes (eigenvectors) of the heat exchanger.

To perform the signal acquisition, a maximum frequency range of up to 1000 Hz was defined. A force-type window was applied to the excitation signal, while an exponential window was used for the response signal. Three samples were used to calculate the average FRF at each impact point. The specifications of the equipment used in the test are described in Table 3.

Table 3. Description of the measurement chain equipment.

Item	Equipment	Manufacturer	Model	Sensibility
1	Signal Analyzer	LMS	Scadas III	-
2	Impact Hammer	PCB	086D05	0,23 mV/N
3	Accelerometer	Ômega	4533-B	9,556mV/g

Given the initial analysis, a second analysis was performed on the movable plate. This time, more measurement points were used, totaling 14 points, aiming for a better representation of the structure's vibration mode. The accelerometer was positioned at measurement point 6 for all impacts. A virtual geometry, shown in Figure 5, was created using the same

coordinates, reference system, and nomenclature as the experimental points in the LMSTest.Lab software, which is responsible for post-processing the modal analysis.

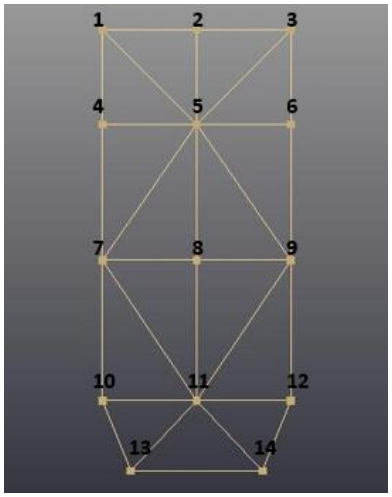

Figure 5. Model of the geometry used for visualization of the modal analysis.

After constructing the geometry, each FRF is indexed to its respective point. In this case, inertances were obtained, which is the ratio of the acceleration signal (response) to the force signal (excitation). The software has an internal routine that generates a summed FRF curve from the measured FRFs. Then, using the Polyreference method available in Test.Lab7a software, modal functions are identified. In the stabilization diagram generated by the software, possible vibration modes are indicated by "s," as seen in Figure 6**.** In addition to vibration frequencies and modal shapes, it is also possible to identify structural damping.

(a) (b)

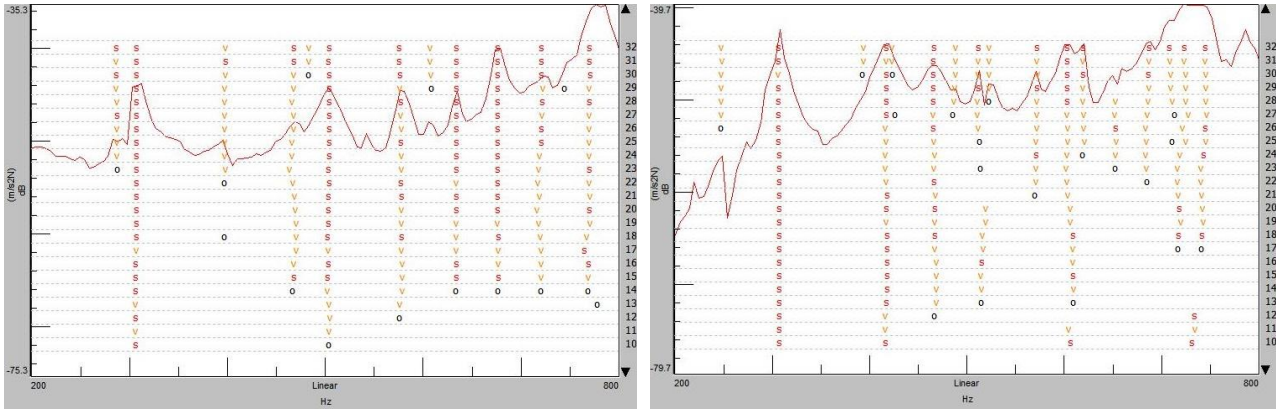

Figure 6. Summed FRF curves obtained in the heat exchanger on the movable plate without reinforcement plate (a) and with reinforcement plate (b), after the stabilization process.

5. RESULTS

5.1 Stresses

Hydrostatic tests on Single and Double configurations of the heat exchanger were conducted up to 10 bar, for the tightening configuration 1A. Figure 7 presents the von Mises stresses obtained for the three configurations in the Single condition (a) and Double condition (b). The von Mises stresses at points SG1, SG2, and SG3 of the plate are plotted against the static pressure of the heat exchanger. Table 4 and Table 5 summarize all stress values for each heat exchanger configuration (I-III) and at each plate location (SG1–SG3), for Single and Double hydrostatic tests, respectively. Stress values are presented for five working pressures (2, 4, 6, 8 and 10 bar). Note that the results from strain gauge SG4, located in the thermal exchange region, were not presented as it had a malfunction.

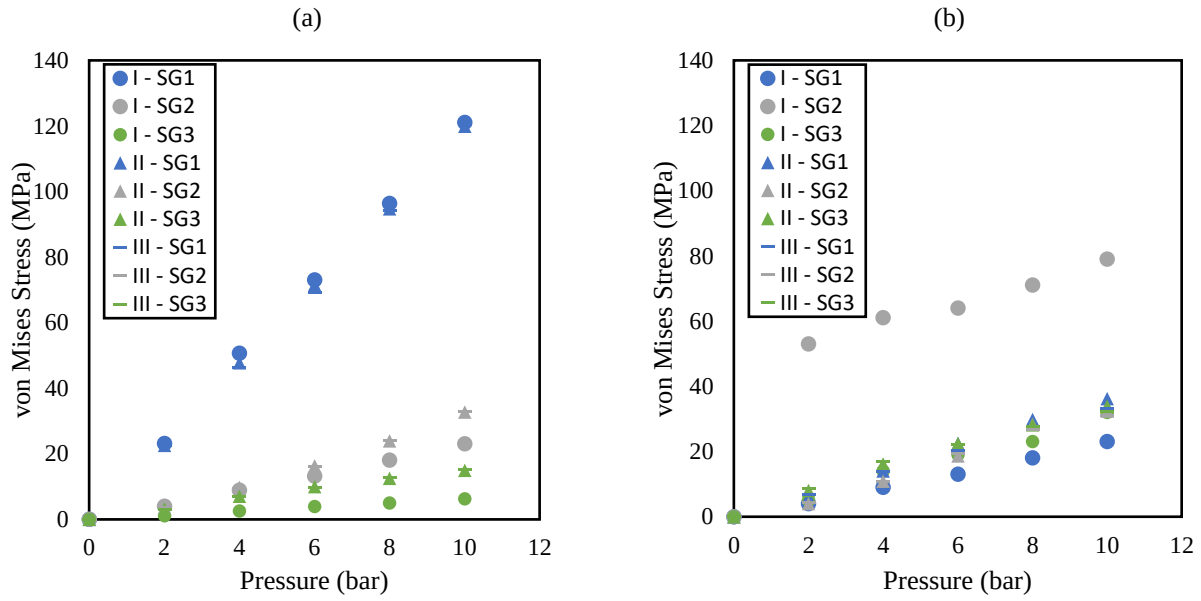

Figure 7. Effect of Single operation (a) and Double (b) operation on von Mises stress levels for the three configurations

Table 4. Effects of single pressurization on von Mises stress levels for the different configurations.

Pressure (bar)	**σ_{VM} (MPa) - Single**								
Configuration	**Distribution area (SG1)**			**Diagonal gasket groove (SG2)**			**Porthole edge (SG3)**		
	I	II	III	I	II	III	I	II	III
2	23	22	23	4	4	4	1	3	3
4	51	48	46	9	10	9	3	7	7
6	73	72	69	13	16	16	4	10	10
8	96	95	94	18	24	24	5	12	13
10	121	120	120	23	33	33	6	15	15

Table 5. Effects of double pressurization on von Mises stress levels for the different configurations.

Pressure (bar)	**σ_{VM} (MPa) - Double**								
Configuration	**Distribution area (SG1)**			**Diagonal gasket groove (SG2)**			**Porthole edge (SG3)**		
	I	II	III	I	II	III	I	II	III
2	4	6	7	53	4	4	5	8	9
4	9	14	14	61	11	11	14	16	17
6	13	22	20	64	19	19	19	22	22
8	18	30	28	71	28	27	23	28	28
10	23	36	33	79	32	31	32	34	32

Stress levels in Table 4 and Table 5 increase with increasing static pressure. They are considerably higher in Single test conditions. When pressurizing a single branch, the pressure difference between the filled branch and the empty one (atmospheric pressure, ~ 1bar) yields plate displacement in the direction of the empty branch. In Double configuration, both branches are pressurized and, therefore, the plate has pressure loads on both faces. Due to the Poisson effect, the plate can expand perpendicularly to the compression load direction. Consequently the local deformation becomes smaller as verified by Martins *et al.* (2022).

When comparing configurations II and III, it is observed that keeping the intermediate plate free or locked does not alter the stress state, with a maximum variation of 3 MPa. Evaluating these configurations together with configuration I, a decrease in stress is observed in the diagonal gasket groove under Double pressurization, reducing from 79 MPa to 32 MPa. However, in the region experiencing the highest mechanical demand, the distribution region (121 MPa), the reinforcement plate has no impact.

5.2 Modal Analysis

In this section, some vibration modes obtained through experimental modal analysis will be presented. Figure 7 shows the FRFs obtained from the heat exchanger (PHE), with and without the presence of the reinforcement plate. The curves obtained from the exploratory tests, with the impact applied to only 5 analysis points on the fixed plate, as well as the curves obtained from the tests on the movable plate, are presented. The normalized amplitude by force is plotted against frequency. Note that the presented curves represent the summation of the measured FRFs during the tests.

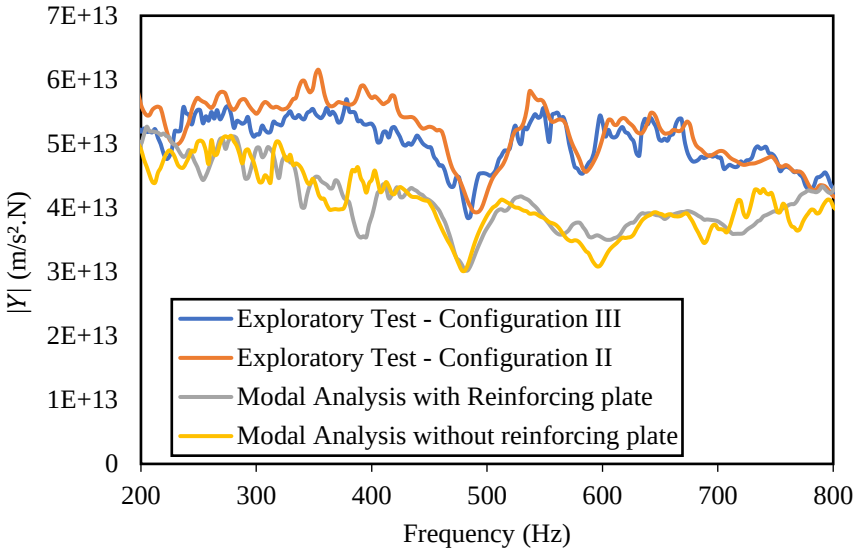

Figure 8. Summed curve of the FRFs obtained from the movable and fixed plates of the heat exchanger (PHE).

In the exploratory tests conducted on the fixed plate, impact procedures were carried out with the reinforcement plate both free and locked. It was observed that the vibration pattern remained unchanged regardless of whether the plate was locked, although more significant peaks were detected at the same frequencies. Therefore, in the tests performed on the movable plate, the PHE was tested only with and without the presence of the reinforcement plate, without considering whether the plate was free or locked.

Overall, the curves exhibit similar behavior, with higher peaks found around 500Hz. These peaks represent the natural vibration frequencies of the system, which correspond to specific vibration modes. The rounded shape of the peaks can be attributed to the slight damping in the system, implying the estimation of damped natural frequencies rather than undamped ones.

The difference in boundary conditions between the fixed plate, which is supported on the ground, and the movable plate does not significantly affect the modal response. It is worth noting that the FRFs obtained from the movable plate, which includes more measurement points, exhibit a greater presence of peaks between the natural frequencies of 200 and 500Hz, providing a more accurate representation of the modal shape of the equipment. Furthermore, the plate constrained by the guides functions as a plate with restricted movements at both ends. Subsequent figures allow the identification of vibration modes at each peak of the FRF obtained through the analysis in Test.Lab7a software.

The pairs of images above represent captures of the plate's motion extremes at the observed frequency, while the other positions of the motion are located between these two points. It is important to note that defining the true boundary conditions for the heat exchanger as a whole is complex. This complexity arises from the fact that the end-plates have movement restrictions at the edges, limited by tie bolts, and the plates are constrained by guide rods in the upper and lower regions. It should be noted that supported-clamped structures may exhibit vibration modes that combine bending and torsion. These modes involve a combination of bending and torsional movements and can be more complex in terms of deformation patterns (João Miguel de Amorin Novais da Costa Nóbrega, 1996; Rao, 2004).

The highest magnitude peak, located around 500Hz, can be correlated with the fundamental vibration mode of a supported-clamped structure. In this mode, the structure forms a bending wave pattern with a node at each end of the plate and an antinode at the center.

At frequencies of 470Hz and 541Hz, as shown in Figure 9b and Figure 9c, respectively, points with lateral displacements are observed, suggesting the presence of torsional components. When exploring higher frequencies, approaching 576Hz (Figure 9d), a complex vibratory behavior emerges. In this range, a combination of higher-order bending modes is evident, characterized by the appearance of multiple nodes and antinodes along the structure. Lateral displacements (torsional) are subtly present in the upper region of the plate. This combination of vibration modes indicates the influence of multifaceted factors, including geometry, boundary conditions, and material properties of the structure.

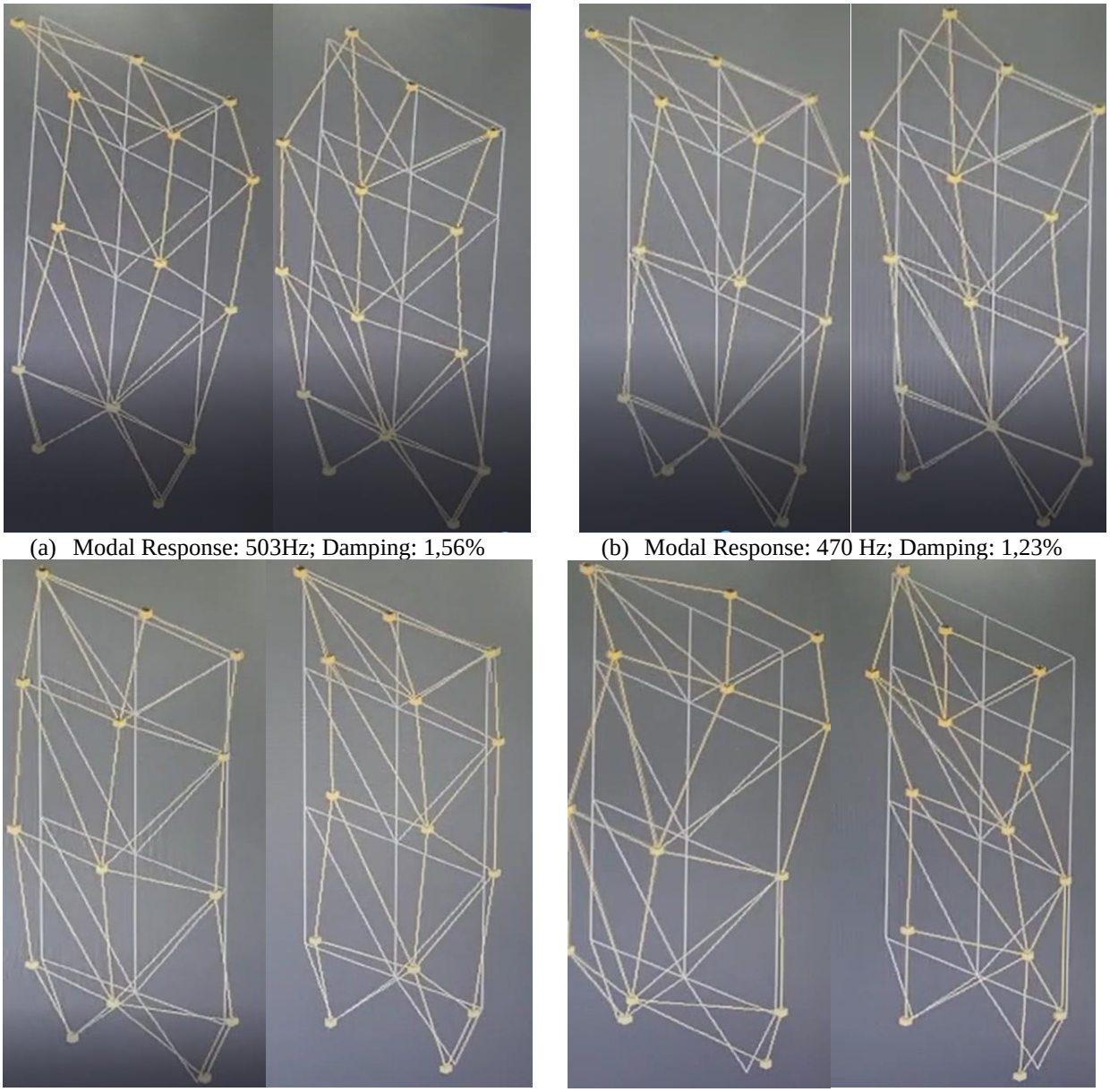

(a) Modal Response: 503Hz; Damping: 1,56%
(b) Modal Response: 470 Hz; Damping: 1,23%
(c) Modal Response: 541Hz; Damping: 0,12%
(d) Modal Response: 576 Hz; Damping: 0,46%

Figure 9. Modes of Vibration in the movable plate of the PHE

In conclusion, the modal analysis highlights remarkable vibrational responses around the mentioned frequencies, demonstrating nuances influenced by the complex support configuration and intrinsic dynamic properties of the structure. For more precise validations, comprehensive modal analyses may be necessary, considering interactive modes and the multifaceted nature of the system.

6. CONCLUSIONS

This article aimed to evaluate the impact of using an intermediate reinforcement plate on the mechanical responses of a PHE-M10 heat exchanger. Based on the results obtained from strain gauge analysis and modal analysis, the following conclusions can be drawn:

The use of a thicker intermediate plate, both in the free and locked condition, minimally alters the stress state of the plate, similar to the case without its presence. The highest stresses predominantly occur in the distribution region in the single condition, regardless of the analysis condition, with magnitudes on the order of 120 MPa at 10 bar pressure.

The reinforcement plate does not significantly alter the modal response, as the observed FRFs are very similar, and in all cases, the first mode of vibration was observed in the frequency range of 500Hz.

Therefore, the observed differences do not justify the use of a 6mm intermediate structural plate, which is ten times thicker than the plates of the heat exchanger, for heat exchangers with fewer than 100 plates and similar dimensions to the studied PHE.

7. REFERENCES

Adolfsson, R., 2016. Life Cycle Assessment and Life Cycle Cost of Heat Exchangers: A Case for Inter Terminals Sweden AB Located in Port of Gothenburg. (Master's thesis). CHALMERS UNIVERSITY OF TECHNOLOGY, Gothenburg, Sweden.
Allemang, R.J., Avitabile, P., 2022. Handbook of experimental structural dynamics. Springer, New York, NY.
Arsenyeva, O., Klemeš, J.J., Kapustenko, P., Fedorenko, O., Kusakov, S., Kobylnik, D., 2021. Plate heat exchanger design for the utilisation of waste heat from exhaust gases of drying process. Energy 233, 121186. https://doi.org/10.1016/j.energy.2021.121186
Beckedorff, L., da Silva, R.P.P., Martins, G.S.M., de Paiva, K.V., Oliveira, J.L.G., Oliveira, A.A.M., 2022. Flow maldistribution and heat transfer characteristics in plate and shell heat exchangers. International Journal of Heat and Mass Transfer 195, 123182. https://doi.org/10.1016/j.ijheatmasstransfer.2022.123182
Carlos Eduardo Prazzo, 2011. Análise Modal de uma Estrutura do Tipo Viga Utilizando Materiais Piezelétricos (PVDF) como Sensores (Dissertação de Mestrado). Universidade Estadual Paulista, São Paulo.
Gut, J.A.W., Pinto, J.M., 2004. Optimal configuration design for plate heat exchangers. International Journal of Heat and Mass Transfer 47, 4833–4848. https://doi.org/10.1016/j.ijheatmasstransfer.2004.06.002
Hewitt, G.F., Shires, G.L., Bott, T.R., 1994. Process heat transfer. CRC Press : Begell House, Boca Raton.
João Miguel de Amorin Novais da Costa Nóbrega, 1996. Modelação de estruturas por análise modal experimental e acoplamento dinâmico (Dissertação de Mestrado). Faculdade de Engenharia da Universidade do Porto, Porto.
Jorge, A.B., Anflor, C.T.M., Gomes, G.F., Carneiro, S.H.D.S. (Eds.), 2022. Fundamental Concepts and Models for the Direct Problem: Volume II in Discrete Models, Inverse Methods, & Uncertainty Modeling in Structural Integrity, 1st ed. Biblioteca Central da Universidade de Brasilia, Brasilia, DF, Brazil. https://doi.org/10.4322/978-65-86503-83-8
Kakaç, S., Liu, H., Pramuanjaroenkij, A., 2020. Heat Exchangers: Selection, Rating, and Thermal Design, 4th ed. CRC Press. https://doi.org/10.1201/9780429469862
Maia, N.M.M., Silva, J.M.M., 2001. Modal analysis identification techniques. Philosophical Transactions of the Royal Society of London. Series A: Mathematical, Physical and Engineering Sciences 359, 29–40. https://doi.org/10.1098/rsta.2000.0712
Martins, G.S.M., Santiago, R.S., Beckedorff, L.E., Possamai, T.S., Oba, R., Oliveira, J.L.G., de Oliveira, A.A.M., Paiva, K.V., 2022. Structural analysis of gasketed plate heat exchangers. International Journal of Pressure Vessels and Piping 197, 104634. https://doi.org/10.1016/j.ijpvp.2022.104634
Rao, S.S., 2004. Vibrações mecânicas, 4. ed.-. ed. Pearson Prentice Hall, São Paulo.
Rydén, L., 2003. Field Reliability of Plate Heat Exchangers in Oil and Gás Process – A Market Perspective (M. Sc. Dissertation). Lund University, Lund, Sweden.
Shah, R.K., Sekuli, D.P., 2003. Fundamentals of Heat Exchanger Design. John Wiley & Sons, Inc., Hoboken, NJ, USA. https://doi.org/10.1002/9780470172605
The American Society of Mechanical Engineers, 2015. ASME Boiler and Pressure Vessel Code - SECTION VIII - Rules for Construction of Pressure Vessels., Alternativa Rules.
Wang, L., Sundén, B., Manglik, R.M. (Eds.), 2007. Plate heat exchangers: design, applications and performance, International series on developments in heat transfer. WIT Press, Southampton ; Boston.
Zahid, F.B., Ong, Z.C., Khoo, S.Y., 2020. A review of operational modal analysis techniques for in-service modal identification. J Braz. Soc. Mech. Sci. Eng. 42, 398. https://doi.org/10.1007/s40430-020-02470-8
Zhang, L., Qian, Z., Deng, J., Yin, Y., 2015. Fluid–structure interaction numerical simulation of thermal performance and mechanical property on plate-fins heat exchanger. Heat Mass Transfer 51, 1337–1353. https://doi.org/10.1007/s00231-015-1507-5

8. RESPONSIBILITY NOTICE

The authors are the only responsible for the printed material included in this paper.